

Single-shot measurement of the orbital-angular-momentum spectrum of partially coherent fields

Girish Kulkarni¹, Rishabh Sahu¹, Omar S. Magaña-Loaiza², Robert. W. Boyd^{2,3}, and Anand K. Jha¹

¹*Department of Physics, Indian Institute of Technology, Kanpur 208016, India*

²*The Institute of Optics, University of Rochester, Rochester, New York 14627, USA*

³*Department of Physics, University of Ottawa, Ottawa, ON, K1N6N5, Canada*

(Dated: January 27, 2023)

We propose an image inversion-based interferometric technique for measuring the orbital-angular-momentum (OAM) spectrum of a field that is an incoherent mixture of OAM eigenstates. The technique directly encodes the angular correlation function of the input field in the azimuthal intensity profile of the output interferogram. We show that for an input field with a symmetric spectrum, a single-shot acquisition of this interferogram is sufficient to measure its OAM spectrum. We first present a proof-of-concept experimental demonstration of this technique for laboratory-produced partially coherent fields with known OAM spectra. We then use this technique to measure the intrinsic OAM spectrum of the signal-idler field from parametric down-conversion over an unprecedented range of more than 150 modes. This technique surpasses all other existing measurement schemes in terms of efficiency and spectral range, and can have significant implications for high-dimensional optical information processing protocols based on the OAM degree of freedom.

An electromagnetic field can be completely specified in terms of the correlations of various orders between the field amplitudes at different spacetime points [1–3]. These correlations encode the spectral content of the field and can be experimentally measured through interference effects manifested by the field [4]. For instance, the temporal correlation function of a light field can be measured in a Mach-Zender interferometer as the visibility profile of the fringes as a function of the temporal delay, from which the frequency spectrum of the input field can be obtained by a Fourier transform.

It is known that much like time and frequency, angular position and orbital angular momentum (OAM) are conjugate physical observables, and consequently the angular position correlation function and the OAM spectrum of a light field are also related by a Fourier transform [5–8]. Moreover, the periodic and continuous character of the angular position variable renders the conjugate OAM basis discrete and infinite-dimensional. This feature makes OAM an attractive degree of freedom for both classical and quantum information-based protocols. Classical communication protocols implemented with OAM mode division multiplexing have been demonstrated to have high channel capacities and spectral efficiencies [9–11]. Quantum communication protocols employing high dimensional quantum states, which can be realized in the OAM degree of freedom, surpass quantum protocols that use low-dimensional states in terms of security [12–14] and bandwidth [15, 16]. Furthermore, OAM-based high-dimensional quantum states can have more efficient gate implementations [17, 18] in quantum computing schemes, and also possess inherent advantages for fundamental tests of quantum mechanics [19–21].

An important problem relevant to several such OAM-based applications is the measurement of the OAM spectrum of a partially coherent field, which in our context

is defined to be an incoherent mixture of more than one OAM eigenstates. The commonly used method is to sequentially project the field into its different constituent OAM eigenstates using computer generated holograms and measure the corresponding intensities [22, 23]. Another technique is an angular analog of the Mach-Zender interferometer in which the field is interfered with a rotated copy of itself, and the visibility profile of the resulting fringes with respect to the rotation angle is obtained [24, 25]. Yet another method involves a Young’s double slit experiment in which the partially coherent field is incident on an aperture consisting of two angular slits, and the visibility of the corresponding fringes is measured as a function of the angular separation between the slits [26, 27]. Since the visibility profile is simply the normalized angular position correlation function itself, the OAM spectrum can be deduced via a Fourier transform. While each of the above techniques have their own advantages, they also individually suffer from issues like sensitivity to noise in fiber-coupling efficiencies, unwanted beam precession introduced by rotary elements, incompatibility with low light levels, etc. Furthermore, these schemes require a sequence of multiple intensity measurements whose number scales with the OAM bandwidth of the partially coherent field.

In this paper, we present an image inversion-based interferometric technique that can measure the OAM spectrum of a partially coherent field in a single-shot measurement. The setup consists of a balanced Mach-Zender interferometer with a disparate number of mirrors in the two arms, which has the action of encoding the angular correlation function of the input field in the azimuthal intensity profile at the output port(s). This technique does not involve any dynamical elements or apertures and is perfectly compatible with low light levels. In what follows, we first present a proof-of-concept experimental

demonstration of this scheme for a partially coherent field with a synthesized rectangular spectrum. Thereafter we employ this technique to measure the OAM spectrum of the partially coherent signal-idler field produced from collinear type-I parametric down-conversion.

We begin with an introduction to the eigenstates of the OAM operator within the paraxial approximation, namely the Laguerre-Gauss (LG) beams [28]. The transverse field amplitudes of these eigenstates can be expressed in the polar co-ordinates by the Laguerre-Gauss functions $LG_l^p(r, \phi)$, which are labelled by an azimuthal index l and a radial index p . These functions have the separable form, $LG_l^p(r, \phi) = f_l^p(r) e^{il\phi}$, where $f_l^p(r)$ is a continuous function of r alone. Therefore, the intensity profile of the beam given by $|f_l^p(r)|^2$ is independent of the azimuthal angle ϕ . The phase profile, given by $e^{il\phi}$, imparts the index l with a physical interpretation as the topological winding number of the phase. It can also be shown that l is a measure of the OAM of the beam and that each photon in such a beam has an OAM of $l\hbar$. For the phase to be single-valued at all azimuthal angles, l is constrained to take on integer values only.

We now consider a partially coherent field which, by our definition, is an incoherently weighted superposition of more than one LG_l^p eigenmodes. Since our goal is only to measure the marginal distribution of the intensities of the constituent pure LG modes with respect to the azimuthal index l , the radial index p is implicitly assumed to be summed over its entire range, and will subsequently be suppressed. If we denote the intensity profile of the partially coherent field by $I(r, \phi)$, then

$$I(r, \phi) = \sum_l S_l |LG_l(r, \phi)|^2, \quad (1)$$

where S_l is defined to be the intensity of the OAM mode with index l and the eigenfunctions $LG_l(r, \phi)$ are normalized as, $\int_0^{2\pi} \int_0^\infty |LG_l(r, \phi)|^2 r dr d\phi = 1$. The quantities S_l for all values of l , together constitute the OAM spectrum of the partially coherent field which we normalize such that $\sum_l S_l = 1$.

The electric field $E_l(r, \phi)$ of the constituent pure LG mode with azimuthal index l takes the general form,

$$E_l(r, \phi) = \sqrt{S_l} f_l(r) e^{il\phi + \tilde{\gamma}_l}, \quad (2)$$

where $\tilde{\gamma}_l$ is a stochastic phase. The resulting superposition of these constituent modes is incoherent if their relative phases are completely random. In other words, the phases $\tilde{\gamma}_l$ must be completely uncorrelated, i.e., $\langle e^{i(\tilde{\gamma}_l - \tilde{\gamma}_{l'})} \rangle = \delta_{ll'}$, where $\langle \dots \rangle$ denotes an average over infinitely many ensemble realizations of the field.

We now consider the physical situation wherein such a partially coherent field is incident into a Mach-Zender interferometer with an odd number of mirrors in one arm and an even number of mirrors in the other arm, such as the one depicted in Fig. (1a). Inspired by previous studies in interferometry and microscopy [29–32], the effect

crucially exploited in this technique is the lateral inversion induced by the mirror on the transverse profile of an incident beam about the axis perpendicular to the plane of incidence. Without loss of generality (see Supplementary Information), we may assume that this inversion axis (IA) defines the origin $\phi = 0$ of the azimuthal angle. The transformation induced by the mirror on the polar co-ordinates is then given by: $r \rightarrow r$ and $\phi \rightarrow -\phi$. This results in the transverse phase profile of a pure LG mode of index l being transformed as $e^{il\phi} \rightarrow e^{-il\phi}$, which as shown in Fig. (1b) effectively amounts to a reversal in the sense of the phase variation. Owing to the disparate number of lateral inversions of the fields in the two arms, the output electric field amplitude $E'_l(r, \phi)$ for that particular mode takes the form,

$$E'_l(r, \phi) = \sqrt{\kappa_1} E_l(r, -\phi) e^{ikd_1} + \sqrt{\kappa_2} E_l(r, \phi) e^{ikd_2}, \quad (3)$$

where we have denoted the path lengths in the two arms as d_1 and d_2 respectively, and k is the magnitude of the wavevector of the beam. The splitting efficiencies of the first and second beam-splitters are $r_1 : t_1$ and $r_2 : t_2$ respectively, and we have defined $\kappa_1 \equiv r_2 t_1$ and $\kappa_2 \equiv r_1 t_2$. For simplicity, we have ignored the phase shifts introduced by reflections at the mirrors and beam-splitters. Using equations (2) and (3), it can now be shown that the intensity profile $I'_l(r, \phi) = \langle |E'_l(r, \phi)|^2 \rangle$, is,

$$I'_l(r, \phi) = S_l |f_l(r)|^2 \left\{ \kappa_1 + \kappa_2 + 2\sqrt{\kappa_1 \kappa_2} \mathbb{V} \cos(2l\phi + \delta) \right\}, \quad (4)$$

where we have defined $\delta \equiv k(d_2 - d_1)$. The parameter $\mathbb{V} \in [0, 1]$ quantifies the temporal coherence for the propagation delay between the fields in the two arms. Thus, we find the output intensity varies sinusoidally with respect to the azimuthal co-ordinate in a floral pattern with $2|l|$ bright fringes, and $2|l|$ dark fringes (as depicted in Fig. (1c) for $l = 4$). Such beams, also referred to as “petal beams”, have been studied in a variety of contexts like quantum metrology, optical trapping, etc [34–39].

Before we proceed further, we issue a clarification pertaining to the notation to be used henceforth. If an index or variable is suppressed from the expression $I'_l(r, \phi)$, then it will be implicit that it has been summed or integrated over its entire range. For instance, it is evident from Eq. (4) that the entire dependence on the OAM index l is in the azimuthal variation of the intensity, while the radial part is simply factored out. Therefore, it is sufficient to restrict our attention to the radially integrated intensity $I'_l(\phi)$ given by, $I'_l(\phi) = \int_0^\infty I'_l(r, \phi) r dr$.

We now recognize that the azimuthal output intensity profile $I'(\phi)$ for the entire partially coherent field as input is simply the incoherent addition of the intensities of the individual interference patterns of each of the constituent pure LG modes. It can be shown that the azimuthal

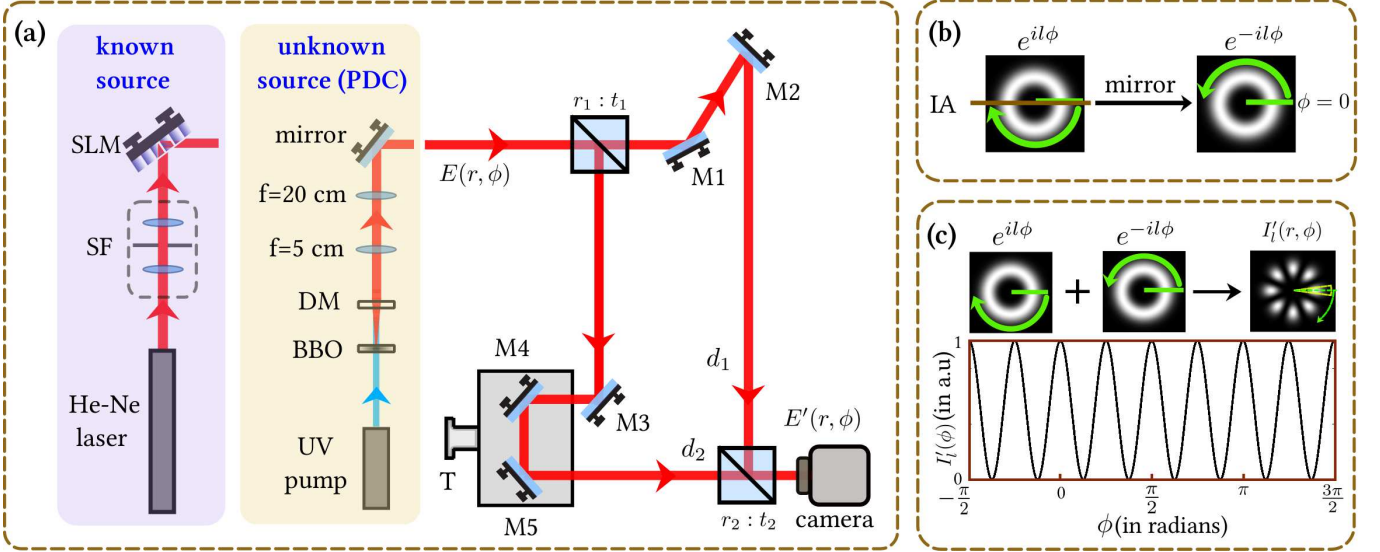


FIG. 1. (color online). We depict in (a) a schematic of the experimental setup featuring a Mach-Zehnder interferometer with an odd and even number of reflections in the two arms. A mirror introduces an image inversion on the transverse profile of a beam about the inversion axis (IA), and consequently the phase profile of the constituent LG mode with index l transforms as $e^{il\phi} \rightarrow e^{-il\phi}$ as shown in (b). Due to the disparate number of such inversions, an interference between these oppositely-varying modes occurs at the second beam-splitter (BS) to produce a floral pattern with $2|l|$ petals for that constituent mode, as shown representatively for $l = 4$ in (c). The interferogram for the entire input field is simply the sum of the floral patterns corresponding to each of the constituent modes, and may be inverted via a Fourier transform to yield the OAM spectrum of the input field. In the first part of the paper, we demonstrate this technique for a known field with a synthesized spectrum. In the second part, we employ the technique to measure the OAM spectrum of the signal-idler field produced from parametric down-conversion. The path lengths, denoted by d_1 and d_2 , lead to a phase difference $\delta = k(d_2 - d_1)$. We denote, SLM: spatial light modulator, SF: spatial filter, DM: dichroic mirror, BBO: type-I beta barium borate crystal, T: translation stage.

profile of the radially integrated output intensity $I'(\phi) = \sum_l I'_l(\phi)$ takes the form,

$$I'(\phi) = \sum_l \frac{S_l}{2\pi} \{ \kappa_1 + \kappa_2 + 2\sqrt{\kappa_1\kappa_2} \mathbb{V} \cos(2l\phi + \delta) \}. \quad (5)$$

Interestingly, this expression can be cast in the more illuminating form,

$$I'(\phi) = \frac{\kappa_1 + \kappa_2}{2\pi} + 2\sqrt{\kappa_1\kappa_2} \mathbb{V} \operatorname{Re} \{ W(\phi, -\phi) e^{i\delta} \}, \quad (6)$$

where we have defined the angular correlation function $W(\phi_1, \phi_2)$ of the input field as,

$$W(\phi_1, \phi_2) = \sum_l \int_0^\infty \langle E_l(r, \phi_1) E_l^*(r, \phi_2) \rangle r dr. \quad (7)$$

As before, $\langle \dots \rangle$ denotes an ensemble average over several realizations of the field. Thus, Eq. (6) states that the angular correlation function of the input field is directly encoded in the azimuthal intensity profile at the output port. More precisely, the azimuthal output intensity $I'(\phi)$ corresponding to the angle ϕ directly measures the correlation between the field at angle ϕ and the field at angle $-\phi$ of the input field. In fact, the function $W(\phi_1, \phi_2)$ is maximum when ϕ and $-\phi$ are the same azimuthal angular position, i.e., $\phi = -\phi$ or $\phi = -\phi + 2\pi$.

As a result, the function $W(\phi, -\phi)$ is encoded in two identical copies, one each centered at the diametrically opposite azimuthal angular positions, $\phi = 0$ and $\phi = \pi$.

We now note an important consequence of the Wiener-Khinchine theorem for stationary random processes. Using Eqs. (2) and (7) it can be shown that,

$$W(\phi_1, \phi_2) = \frac{1}{2\pi} \sum_l S_l e^{il(\phi_1 - \phi_2)}. \quad (8)$$

In other words, the angular correlation function of the partially coherent input field is related to its OAM spectrum by a Fourier relation. This can be understood by recognizing that a partially coherent field can be thought of as a wide-sense-stationary random process with respect to the azimuthal angle [40]. It then follows from Eqs. (6) and (8) that values of S_l can be deduced from the azimuthal intensity $I'(\phi)$ using the relation,

$$S_l = \frac{1}{2\mathbb{V}\sqrt{\kappa_1\kappa_2}} \int_0^{2\pi} \left(I'(\phi) - \frac{\kappa_1 + \kappa_2}{2\pi} \right) \times \left(\frac{\cos 2l\phi}{\cos \delta} - \frac{\sin 2l\phi}{\sin \delta} \right) d\phi. \quad (9)$$

It may be noted that the spectrum can be deduced for any value of \mathbb{V} and δ , except for pathological conditions such as $\mathbb{V} = 0$, or δ taking an odd multiple of $\pi/2$. However,

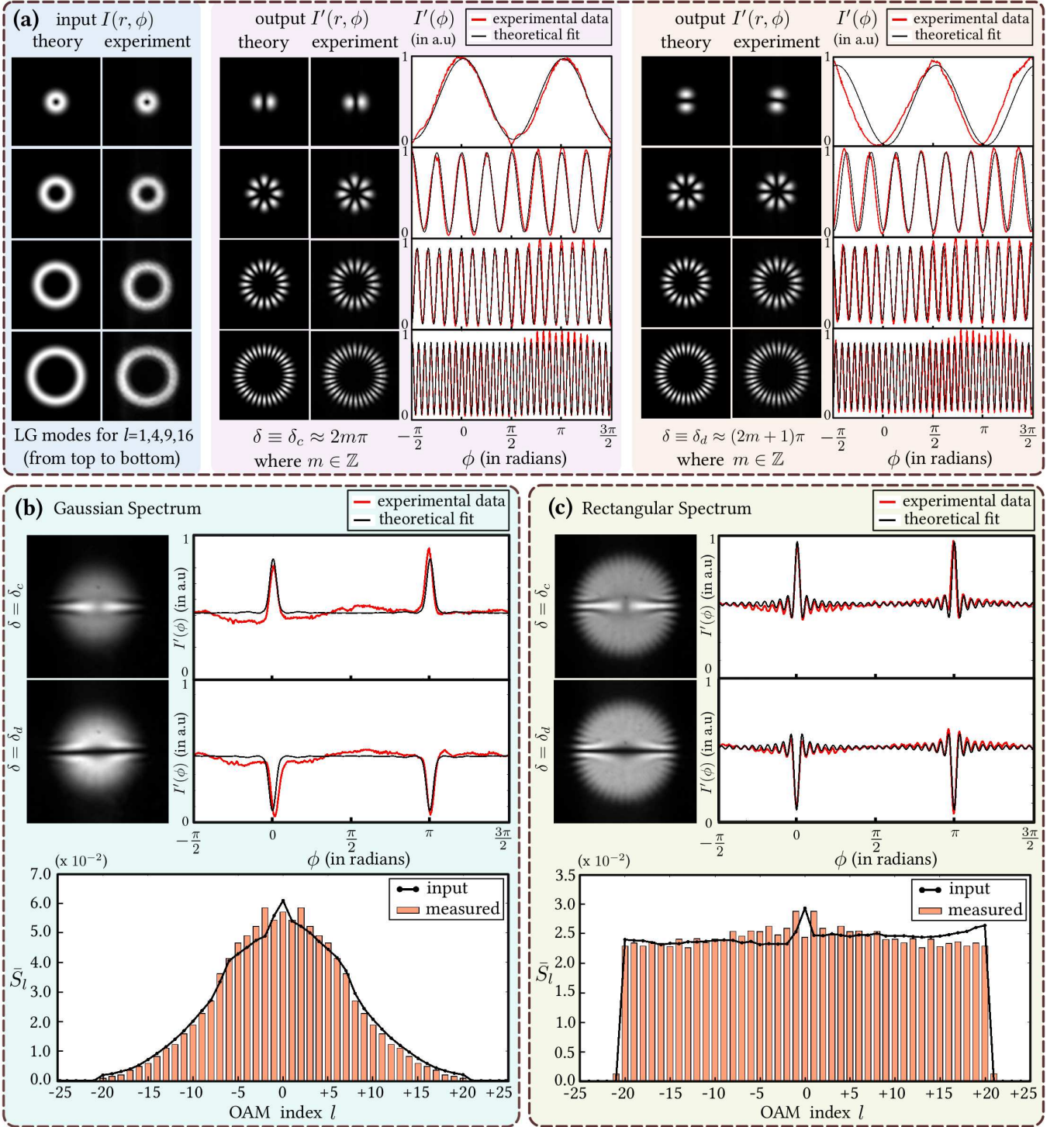


FIG. 2. (color online). We present results from a proof-of-concept demonstration of this measurement technique using input fields synthesized using the SLM. In (a.), we depict the experimental and theoretical images of a few representative *LG* modes with indices $l = 1, 4, 9$, and 16 as input fields and their corresponding output interferograms for the two optimal values of δ : $\delta = \delta_c$ which is close to an even multiple of π , and $\delta = \delta_d$ which is close to an odd multiple of π . Notice that the measured interferograms for OAM mode with index l as input consist of floral interference patterns with $2|l|$ fringes, with bright (dark) fringes centered at $\phi = 0$ and $\phi = \pi$ for $\delta = \delta_c$ ($\delta = \delta_d$). The corresponding radially integrated azimuthal intensities $I'(\phi)$ show a sinusoidal variation with a maxima (minima) at $\phi = 0$ and $\phi = \pi$ for $\delta = \delta_c$ ($\delta = \delta_d$). In (b). and (c)., we depict the output interferograms and azimuthal output intensities $I'(\phi)$ for partially coherent fields with a Gaussian and rectangular spectrum respectively, obtained by accumulating the floral patterns for the constituent *LG* modes in the corresponding weightages. Notice the angular correlation functions of the input fields with Gaussian and Sinc profiles in the azimuthal output intensity plots at the angles $\phi = 0$ and $\phi = \pi$, appearing constructively for $\delta = \delta_c$, and destructively for $\delta = \delta_d$. The inferred spectra for these values of δ are averaged to yield the measured spectrum \bar{S}_l , which are depicted in the bar plots in (b). and (c). Thus, the scheme is able to measure the spectrum in both cases to a good accuracy. The noise present may be attributed to two factors: the asymmetry in the input spectrum, and aberrations in the generated *LG* modes due to imperfections of the SLM.

it is evident from the above expressions that the values of \mathbf{V} , $\cos \delta$ and $\sin \delta$ are required in order to carry out the above integration. Now if the field is quasimonochromatic, the parameter \mathbf{V} can be made close to unity by setting the path length difference $d_2 - d_1$ to be much smaller than the temporal coherence length. The value of $\cos \delta$ can be inferred directly from Eq. (5) as,

$$\cos \delta = \frac{\pi}{\mathbf{V} \sqrt{\kappa_1 \kappa_2}} \left(I'(0) - \frac{\kappa_1 + \kappa_2}{2\pi} \right), \quad (10)$$

which in turn yields the value of $\sin \delta$, but only upto an overall sign. This latter caveat reveals a noteworthy feature of this interferometer. Notice that under the combined transformation of $\delta \rightarrow -\delta$ and $l \rightarrow -l$, Eq. (5) and consequently Eq. (9) remain unchanged. Intuitively, this may be understood by recognizing that the action of the interferometer on a pure *LG* mode with index l is identical to the action of the interferometer with its arms interchanged, on a pure *LG* mode with index $-l$. The implication of this feature for the measurement scheme is that in the absence of prior information or an additional measurement that ascertains the sign of $\sin \delta$, the spectrum S_l can be inferred only upto a parity flip. In other words, a single-shot measurement yields both S_l and S_{-l} as possible spectrums of the partially coherent field. This feature is not too restrictive because the missing information of δ can always be obtained from a few additional measurements, whose number does not scale with the OAM bandwidth. Fortunately, this is usually unnecessary since most partially coherent fields commonly of interest do not carry an overall OAM, i.e, they have a symmetric OAM spectrum. For such fields, the above degeneracy of solutions is irrelevant since $S_l = S_{-l}$. In what follows, we shall focus our attention only on fields with a symmetric spectrum, in which case the term with the sine function in Eq. (9) can be ignored. We now present our experimental results for a proof-of-concept demonstration of this measurement scheme.

In the experiment, a 632-nm wavelength He-Ne laser beam was spatially filtered and incident on a spatial light modulator (SLM) as shown in source Fig. (1a). Using the method of Arrizon *et al.* [41], we generated holograms to produce pure *LG* modes from $l = -20$ to $l = +20$ with controllable weightages in the first diffraction order. The produced *LG* beam is incident into the depicted Mach-Zender interferometer, in which the path-difference phase δ was adjustable using the translation stage. The output interferogram at the second beam-splitter is then imaged in a single-shot acquisition using an EMCCD camera and normalized with respect to the total intensity of the incoming field. The azimuthal intensity $I'(\phi)$ is obtained by evaluating the total number of counts in a thin angular cakeslice placed at the angle ϕ and integrated upto a radius slightly greater than the beam radius.

As shown in Fig. (2a), the output interferograms for the pure *LG* modes as input consist of floral interference

patterns with $2|l|$ petals, where l is the OAM index of the mode. The floral patterns for pure *LG* modes from $l = -20$ to $l = +20$ were individually recorded. In order to simulate the interferogram for a partially coherent input field with Gaussian and rectangular spectra from $l = -20$ to $l = +20$, all the respective floral patterns are accumulated incoherently by manipulating the phase patterns on the SLM to ensure the required weightages. As observed in Figs. (2b) and (2c), when $\delta \equiv \delta_c$ is nearly equal to an even multiple of π , there is a constructive overlap of bright fringes at $\phi = 0$ and $\phi = \pi$ for all the floral patterns, resulting in the angular correlation function peaking upwards at $\phi = 0$ and $\phi = \pi$. In contrast when $\delta \equiv \delta_d$ is nearly equal to an odd multiple of π , all the floral patterns destructively overlap on dark fringes at $\phi = 0$ and $\phi = \pi$, causing the angular correlation function to dip downwards.

Note from Eqs. (9) and (10) that while in principle we can infer the input OAM spectrum from the azimuthal intensity profile for any value of δ , we have focused on the situations of $\delta = \delta_c$ and $\delta = \delta_d$ being close to an even or odd multiple of π respectively due to their optimal signal-to-noise ratio. Now it can be shown that the noise for non-zero l originating from normalization errors, imprecise knowledge of the parameters κ_1, κ_2 and \mathbf{V} can be practically eliminated by evaluating \bar{S}_l , which is the average of the spectra inferred from the azimuthal intensities corresponding to $\delta = \delta_c$ and $\delta = \delta_d$ respectively. It must be noted however that this two-shot averaging procedure does not eliminate the error in the measured value \bar{S}_0 corresponding to $l = 0$ unless the additional condition $\cos \delta_c = -\cos \delta_d$ is satisfied (See Supplementary Information for more detail).

In Fig. (2b) and (2c), we depict our measurements for the artificially simulated partially coherent fields with a Gaussian and rectangular spectrum respectively. Notice that the measured spectrum \bar{S}_l averaged over the single-shot measurements for $\delta = \delta_c$ and $\delta = \delta_d$ is able to reproduce the input spectrum to a good degree of fidelity. Now note that while our measurement assumes a symmetric input spectrum, the experimentally generated input spectrum is mildly asymmetric. Moreover, there are lop-sided aberrations in the generated pure *LG* modes, especially for higher values of l . As seen in figures (2b) and (2c), these imperfections contribute to noise in the measured spectrum. However since these issues pertain to the fidelity of the simulation of the input field and not to some intrinsic limitations of the technique, the noise in the measurement of a true partially coherent field with a symmetric spectrum is expected to be lower. We have confirmed this expectation for numerically simulated partially coherent fields, for which the measurements have yielded an almost-perfect match with the input spectrum. We now turn our attention to a naturally generated partially coherent field, namely the signal-idler field produced in parametric downconversion (PDC).

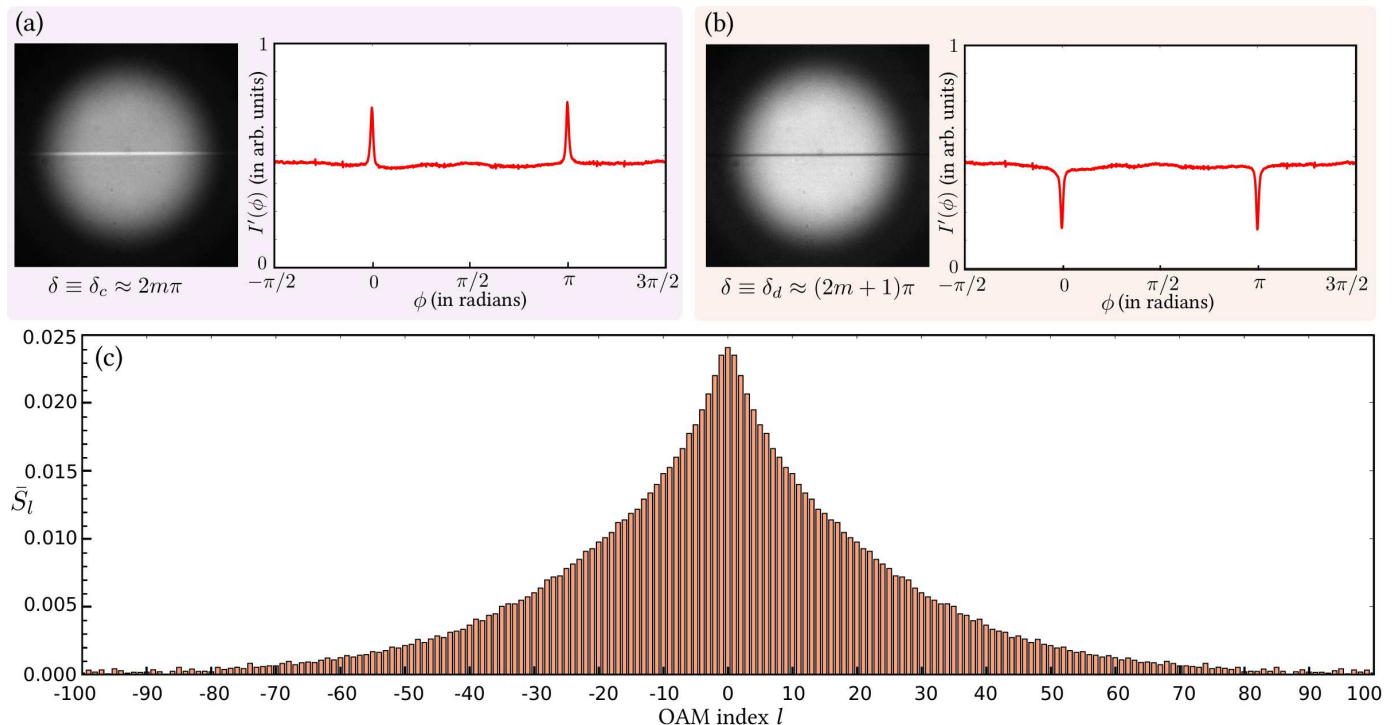


FIG. 3. (color online). We present experimental observations for the signal-idler field produced from PDC. The images and azimuthal intensity plots in (a). and (b). correspond to interferograms obtained for $\delta = \delta_c$ and $\delta = \delta_d$ respectively. We observe the angular correlation function of the signal-idler field centered at the angular positions $\phi = 0$ and $\phi = \pi$ to have a near-Lorentzian profile. In (c)., we present the average measured spectrum \bar{S}_l from the two interferograms, which shows a nearly-exponential profile. The technique does not discard or post-select any part of the field, making this the first measurement of the intrinsic spectrum of the signal-idler field over such a wide range of OAM eigenstates.

The process of PDC involves a pump photon which is annihilated via an interaction with a nonlinear crystal to produce a pair of entangled photons, termed as signal and idler [42]. For experiments restricted to one-photon detection, it can be shown that by virtue of conservation of OAM, the field comprising these photon pairs can be described as an incoherent mixture of OAM eigenstates [43, 44]. In fact, the width of the OAM spectrum of this signal-idler field is related to the OAM entanglement in the two-photon state [46, 47]. However in order to gain information about the latter, it is necessary to measure the intrinsic OAM spectrum of the entire signal-idler field generated in the process, and not some post-selected portion of it. To the best of our knowledge, this challenge has been met so far by only one experiment, which measured the OAM spectrum over a range of about fifty modes from a sequence of coincidence measurements for different configurations of a rotary element [48]. Now note that the single-shot technique of the present study does not inherently involve any post-selection. Moreover, the range of the OAM spectrum measurement is only limited by the sensor element size of the camera. We now therefore undertake the task of measuring the intrinsic OAM spectrum of the signal-idler field produced from PDC using the single-shot technique.

In our experiment, as depicted in Fig. (1), an ultra-violet (UV) continuous-wave pump laser of beam radius 1 mm and Gaussian transverse mode profile is incident on a type-I beta barium borate (BBO) crystal of 2 mm thickness with conditions met to ensure collinear down-conversion. The generated signal-idler field is separated from the residual pump photons using a dichroic mirror (DM). Thereafter, the field passes through a pair of lenses whose collection angle is much larger than the typical emission cone angle of the downconverted field expected for the setup parameters [45]. This ensures that no part of the incoming field is post-selected out from the measurement procedure and the resulting interferogram from the entire field is imaged on the EMCCD camera. We depict the two representative interferograms corresponding to the two optimal situations of δ in Figs. (3a) and (3b). We clearly observe the angular correlation function encoded in the azimuthal intensity profiles at $\phi = 0$ and $\phi = \pi$, peaking upwards for $\delta = \delta_c$ and dipping downwards for $\delta = \delta_d$. The average spectrum inferred from these interferograms is depicted in Fig. (3c). It suggests a nearly-exponential spectrum spanning more than a hundred and fifty OAM eigenstates. This corresponds to the first ultra-broadband measurement of the intrinsic OAM spectrum of the signal-idler field from PDC.

DISCUSSION

In this article, we have proposed and implemented an interferometric technique that can measure the OAM spectrum of a partially coherent field over a wide range of OAM eigenstates using just a single-shot acquisition. From the standpoint of practical applicability, we expect that the high efficiency and ease of implementation of this technique would make it the ideal choice for optical information processing applications that employ OAM-spectrum measurements as part of their protocols. The unparalleled spectral range of measurement offered by this technique can boost the scalability and performance of such applications. From a fundamental perspective, this technique can now enable the experimental measurement of OAM-entangled two-photon states with very large Schmidt dimensionality. As a result, this technique could lead to major advances in our understanding of high-dimensional OAM entanglement in optical fields. We finally expect that the concept of image-inversion crucially exploited in this technique, can be employed in more general settings to probe correlation properties and spectral characteristics of light fields in other degrees of freedom.

METHODS

Prior to the experiment, the interferometer needs to be characterized by measuring the splitting ratios of the beam-splitters. After the experiment is set up, we block one arm of the interferometer and measure the total intensity recorded at the output. We then divide this intensity by the appropriate splitting coefficient to obtain the total intensity of the input field to the interferometer. The total input intensity will be used to normalize the interferograms recorded using the camera.

In order to obtain an interferogram with high visibility, the path-length difference can be tuned using the translation stage to be within the temporal coherence length of the input field. In order to ensure that $\delta \equiv \delta_c$ is approximately an even multiple of π , we tune the translation stage upto the point where the angular correlation function is oriented upwards with maximum height above the flat pedestal. After the acquisition of the interferogram, the condition $\delta \equiv \delta_d$ being approximately an odd multiple of π can be achieved in either of the two following ways: (i). starting from the position $\delta = \delta_c$, introduce a dynamical or geometric phase of π manually by means of precise translations or waveplates, or (ii). if such precise control is not available, then it suffices to select the interferogram with the angular correlation function oriented downwards but with the depth approximately equal in magnitude to the height of the correlation function from the $\delta = \delta_c$ interferogram. Both these methods ensure that δ_c and δ_d are roughly com-

plementary, i.e. $\cos \delta_c \approx -\cos \delta_d \approx 1$ which ensures an almost perfect noise cancellation in the measured spectrum. Note that any error introduced in this procedure will only affect the $l = 0$ component of the measured OAM spectrum, while the nonzero l components differ from the true values only by a common scaling factor.

In order to obtain the azimuthal intensities from the acquired images of the interferograms, we first scale up the images by a factor of eight using a bicubic interpolation method. This mitigates the discretization errors introduced due to pixelation of the images. In order to evaluate the azimuthal intensity $I'(\phi)$, we position a thin angular cakeslice (depicted in Fig. (1c) at $\phi = 0$) at the angle ϕ and evaluate the total number of intensity counts in the region. The positioning of the cakeslices must be done accurately so that they trace out the transverse beam profile exactly from the center of the beam. The number of cakeslices required increases as the number of modes in the partially coherent field increases. For our purposes, it sufficed to have about a thousand cakeslices trace the interferogram over the entire azimuthal range.

-
- [1] *Optical Coherence and Quantum Optics*, L. Mandel, E. Wolf, Cambridge University Press (1999).
 - [2] R. J. Glauber, Phys. Rev. **130**, 2529, (1963).
 - [3] E. C. G. Sudarshan, Phys. Rev. Lett. **10**, 277, (1963).
 - [4] R. J. Glauber, Phys. Rev. Lett. **10**, 84, (1963).
 - [5] S. M. Barnett and D. T. Pegg, Phys. Rev. A **41**, 3427 (1990).
 - [6] E. Yao, S. Franke-Arnold, J. Courtial, S. M. Barnett, and M. J. Padgett, Opt. Express **14**, 9071, (2006).
 - [7] A. K. Jha, B. Jack, E. Yao, J. Leach, R. W. Boyd, G. S. Buller, S. M. Barnett, S. Franke-Arnold, and M. J. Padgett, Phys. Rev. A **78**, 043810 (2008).
 - [8] B. Jack, M. Padgett, and S. Franke-Arnold, New J. Phys. **10** 103013 (2008).
 - [9] J. Wang, J. Yang, I. M. Fazal, N. Ahmed, Y. Yan, H. Huang, Y. Ren, Y. Yue, S. Dolinar, M. Tur and A. E. Willner, Nat. Phot. **6**, 488496 (2012).
 - [10] N. Bozinovic, Y. Yue, Y. Ren, M. Tur, P. Kristensen, H. Huang, A. E. Willner, S. Ramachandran, Science **340**, 6140, (2013).
 - [11] Y. Yan, G. Xie, M. P. J. Lavery, H. Huang, N. Ahmed, C. Bao, Y. Ren, Y. Cao, L. Li, Z. Zhao, A. F. Molisch, M. Tur, M. J. Padgett & A. E. Willner, Nat. Comm. **5**, 4876 (2014).
 - [12] K. Karimipour, A. Bahraminasab, and S. Bagherinezhad, Phys. Rev. A **65**, 052331 (2002).
 - [13] N. J. Cerf, M. Bourennane, A. Karlsson, and N. Gisin, Phys. Rev. Lett. **88**, 127902 (2002).
 - [14] G. M. Nikolopoulos, K. S. Ranade and G. Alber, Phys. Rev. A **73**, 032325 (2006).
 - [15] M. Fujiwara, M. Takeoka, J. Mizuno, and M. Sasaki, Phys. Rev. Lett. **90**, 167906 (2003).
 - [16] J. Cortese, Phys. Rev. A **69**, 022302 (2004).
 - [17] T. C. Ralph, K. Resch, and A. Gilchrist, Phys. Rev. A **75**, 022313 (2007).

- [18] B P. Lanyon, M. Barbieri, M. P. Almeida, T. Jennewein, T. C. Ralph, K. J. Resch, G. J. Pryde, J. L. O'Brien, A. Gilchrist and A. G. White, *Nature Physics* **5**, 134 - 140 (2009).
- [19] D. Kaszlikowski, P. Gnacinski, M. Zukowski, W. Miklaszewski, and A. Zeilinger, *Phys. Rev. Lett.*, **85**, 4418 (2000).
- [20] D. Collins, N. Gisin, N. Linden, S. Massar and S. Popescu, *Phys. Rev. Lett.* **88**, 040404 (2002).
- [21] T. Vetsi, S. Pironio, and N. Brunner, *Phys. Rev. Lett.* **104**, 060401 (2010).
- [22] A. Mair, A. Vaziri, G. Weihs, and A. Zeilinger, *Nature (London)* **412** 313 (2001).
- [23] G. Gibson, J. Courtial, M. J. Padgett, M. Vasnetsov, V. Pasko, S. M. Barnett, and S. Franke-Arnold, *Opt. Exp.* **12**, 22 (2004).
- [24] R. Zambrini and S. M. Barnett, *Phys. Rev. Lett.* **96**, 113901 (2006).
- [25] H. D. L. Pires, J. Woudenberg, and M. P. van Exter, *Opt. Lett.* **35** 889 (2010).
- [26] M. Malik, S. Murugkar, J. Leach, R. W. Boyd, *Phys. Rev. A* **86** (6), 063806 (2012).
- [27] A. K. Jha, G. S. Agarwal, and R. W. Boyd, *Phys. Rev. A* **84** 063847 (2011).
- [28] L. Allen, M. W. Beijersbergen, R. J. C. Spreeuw, and J. P. Woerdman, *Phys. Rev. A* **45**, 8185 (1992).
- [29] C. Iaconis, I. A. Walmsley, *Opt. Lett* **21** 1783-1785 (1996).
- [30] M. Santarseiro and R. Borghi, *Opt. Lett* **31** 861-863 (2006).
- [31] K. Wicker, S. Sindbert, and R. Heintzmann, *Opt. Exp.* **17** 15491-15501 (2009).
- [32] D. Weigel, H. Babovsky, A. Kiessling, R Kowarschik, *Opt. Comm.* **284** 2273-2277 (2011).
- [33] *Introduction to the Theory of Coherence and the Polarization of Light*, E. Wolf, Cambridge University Press (2007).
- [34] M. P. MacDonald, L. Paterson, K. Volke-Sepulveda, J. Arlt, W. Sibbett, and K. Dholakia, *Science* **296**, 1101 (2002).
- [35] A. Jesacher, S. Fr uhpapter, S. Bernet, and M. Ritsch-Marte, *Opt. Express* **12**, 4129 (2004).
- [36] S. Franke-Arnold, J. Leach, M. J. Padgett, V. E. Lembessis, D. Ellinas, A. J. Wright, J. M. Girkin, P. Ohberg, and A. S. Arnold, *Opt. Express* **15**, 8619 (2007).
- [37] C. H. J. Schmitz, K. Uhrig, J. P. Spatz, and J. E. Curtis, *Opt. Express* **14**, 6604 (2006).
- [38] V. D'Ambrosio, N. Spagnolo, L. Del Re, S. Slussarenko, Y. Li, L. Chuan Kwek, L. Marrucci, S. P. Walborn, L. Aolita and F. Sciarrino, *Nat. Comm.* **4**, 2432 (2013).
- [39] P. Wozniak, P. Banzer, F. Bouchard, E. Karimi, G. Leuchs, R. W. Boyd, *Phys. Rev. A* **94**, 021803(R) (2016).
- [40] *Statistical Optics*, J. W. Goodman, John Wiley and Sons, (2015).
- [41] V. Arrizon, U. Ruiz, R. Carrada, and L. A. Gonzalez, *J. Opt. Soc. Am. A* **24**, 3500-3507 (2007).
- [42] D. C. Burnham and D. L. Weinberg, *Phys. Rev. Lett.* **25**, 84 (1970).
- [43] S. P. Walborn, A. N. de Oliveira, R. S. Thebaldi, and C. H. Monken, *Phys. Rev. A* **69**, 023811 (2004).
- [44] S. Franke-Arnold, S. M. Barnett, M. J. Padgett, and L. Allen, *Phys. Rev. A* **65**, 033823 (2002).
- [45] P. G. Kwiat, E. Waks, A. G. White, I. Appelbaum, and P. H. Eberhard, *Phys. Rev. A* **60** 773 (1999)
- [46] J. P. Torres, A. Alexandrescu, and Lluís Torner, *Phys. Rev. A* **68**, 050301 (2003).
- [47] C. K. Law and J. H. Eberly, *Phys. Rev. Lett.* **92**, 127903 (2004).
- [48] H. Di Lorenzo Pires, H. C. B. Florijn, and M. P. van Exter, *Phys. Rev. Lett.* **104**, 020505 (2010).